Facilitating Lunar Operations: The Laser Sintering Robotic Hexapod Mission

Cade May*, Laith Bader*, Claire Brandon*, Jacob Bui*, and Justin Wade*
Auburn University, Auburn, Alabama, 36830

Recent increased interest in returning humans to the lunar surface and ultimately the Martian surface has led to a need for developing efficient construction technologies in extraterrestrial environments. In-situ resource utilization (ISRU) has been widely identified as a crucial field to develop to reduce mission costs and increase long-term mission sustainability. The Laser Sintering Robotic Hexapod (LSRH) mission presented in this work is designed to use laser sintering technology to autonomously create a launch and landing pad (LLP) from lunar regolith. The primary benefits of LLP construction include dust mitigation and increased stability upon launch and landing, increasing the chance of mission success. An incremental construction method, whereby individual tiles are constructed over several days and combined to form an entire pad, is planned due to mission constraints. The mission goal is to construct an 18-meter LLP to support medium-sized lunar landers. A hexapod mobility system was chosen to support this effort. This mobility system will provide stability and greater opportunity for complex laser sintering patterns. Most importantly, this mobility system will prove the technology in the lunar environment, thus supporting the goal of fostering "Extreme Access" that is stated within the NASA Moon to Mars Architecture. The LSRH is planned to be transported onboard the Astrobotic Griffin Lander and reliant upon the craft for power generation and communication. Key technologies identified within this work include laser sintering technology and hexapod control systems. A prototype is currently being developed to prove the feasibility of a hexapod mobility system.

Nomenclature

a	=	Side Length
A_{hex}	=	Area of a Hexagon
D_{beam}	=	Beam Diameter
d_{spot}	=	Spot Diameter
$E_{surface}$	=	Areal Energy Density
f	=	Focal Length of Focusing Lens
f_c	=	Focal Length of Collimating Lens
h	=	Hatch Spacing
M	=	Beam Quality Factor
t	=	Time
θ	=	Numeric Aperture
λ	=	Wavelength
v	=	Scanning Speed

Key Acronyms

AULUNA	=	Astronautics Union for Lunar and Near-space Advancement
ESA	=	European Space Agency
ETF	=	Environmental Test Facility

*Undergraduate, Department of Aerospace Engineering, Auburn University, Auburn AL

IK	=	Inverse Kinematics
ISRU	=	In-Situ Resource Utilization
JSC	=	Johnson Space Center
LiDAR	=	Light Detection and Ranging
LLP	=	Launch and Landing Pad
LRT	=	Lunar Regolith Terrain
LSRH	=	Laser Sintering Robotic Hexapod
MSFC	=	Marshall Space Flight Center
NASA	=	National Aeronautics and Space Administration
RASSOR	=	Regolith Advanced Surface Systems Operations Robot
VIPER	=	Volatiles Investigating Polar Exploration Rover

I. Introduction

A current focus of the aerospace industry is to return humans to the Moon. Recent initiatives to return to the lunar surface such as Artemis [1] and Blue Ghost [2] have revealed many challenges facing lunar operations. One such challenge is the issue of dust mitigation. Lunar regolith is highly porous and composed of jagged particles spanning a wide size range, making it extremely abrasive. In addition, regolith can contain oxidized iron that contributes to electrostatic charging. With the Moon's low gravity and lack of atmosphere, charged dust can remain lofted and mobile. When high-thrust rocket plumes impinge on the surface, regolith can be ejected at high velocities and dispersed over long distances, increasing the risk of erosion, contamination, and damage to nearby assets. To better support future lunar operations, mitigating plume-driven dust and surface degradation is a critical challenge. In addition to dust mitigation, stability is also a critical challenge. Providing a flat, stable ground for landing is also of utmost importance for missions involving expensive equipment or human life. Lunar landers, such as the Odysseus Moon Lander from Intuitive Machines [3], have tipped over while landing, highlighting the need for stable landing platforms. A promising solution to the dust mitigation and stability issues that has emerged in literature is to build launch and landing pads (LLPs) for spacecraft [4]. This paper proposes a mission for a robotic hexapod, equipped with a laser sintering arm, to build an LLP on the lunar surface.

Detailed research on the subject of laser sintering is available [5]. Most available research focuses on small-scale applications, such as the MOONRISE rover from the ESA that can laser sinter on a two-dimensional scale [6]. However, a pathway to larger-scale applications has been demonstrated; NASA configured a laser sintering system that can build three-dimensional structures with regolith simulants [7].

Future utilization of the lunar and martian surfaces will require vehicles to traverse hazardous terrain. According to NASA's Lunar Surface Innovation Initiative under the Space Technology Mission Directorate, a key goal of technological development is to foster "Extreme Access" [8]. While mostly reliable mobility systems have been implemented for missions with rather basic mobility requirements, these systems will be inadequate for missions with more challenging mobility requirements. Therefore, providing a resilient and adaptable mobility system will provide much-needed assurance for future missions. The hexapod design is one such mobility system. This mobility system, though presenting challenges in controls engineering, has received increasing interest in literature [9] [10]. While the hexapod is not a brand-new concept, the idea of putting it on the Moon is novel. Cost-benefit analyses of hexapods exist in literature, but limited information concerning hexapods traversing regolith simulants is available [11]. This mission aims to prove the utility of the hexapod mobility system on the Moon. The laser sintering mission has relatively simple mobility requirements, meaning that the hexapod system can be proven as a viable technology while performing another task (i.e., laser sintering LLPs). The hexapod will also enable the laser sintering operation to accommodate a wide variety of potential sintering patterns, allowing for greater versatility in accomplishing the most important objective.

This document begins with an overview of the LSRH system, including an identification of constraints and objectives. A discussion on the lunar environment follows, with a detailed discussion of the LSRH's mobility system coming next. The work finishes with a risk assessment and conclusion.

II. Mission Overview

The goals of the LSRH mission focus on ISRU operations and proving novel technology. The primary objectives of the mission are as follows:

1) Autonomously construct one 18-meter diameter LLP for future spacecraft use

2) Demonstrate the feasibility and utility of a hexapod mobility system in the lunar environment

The choice of an 18-meter LLP is based upon a key analysis available in literature regarding the optimal landing pad size for a medium-sized 50 ton lander [12], similar in size to the Blue Moon lander [13]. This mission is in line with the objectives of the Artemis campaign [1]. Secondary objectives are also identified for further mission goals. The secondary objectives of the mission are as follows:

1) In the event of system underperformance, construct one 10-meter diameter LLP for future spacecraft use
2) Demonstrate the ability of autonomous systems in constructive lunar activities

The concept of operations for the LSRH mission is shown in Figure 1. The LSRH will travel on board the Astrobotic Griffin Lander from the Earth to the lunar surface. The target location for landing will be near the south pole of the Moon: Nobile Rim 2. The choice of this landing location will be further explained in subsequent sections. After landing, the LSRH will carefully and autonomously descend the Griffin's unloading ramp. A tethered power cable connection to the Griffin will provide a large source of continuous power for the mission. The LSRH will then maneuver sufficiently away from the Griffin and begin the laser sintering operation. The LLP will be constructed incrementally, with individual 1-meter hexagons combining to form the entire landing pad. During the lunar night, the LSRH will enter a hibernation state to maintain heat. The Griffin contains ample power storage to support this state during a relatively short lunar night due to its location near the south pole.

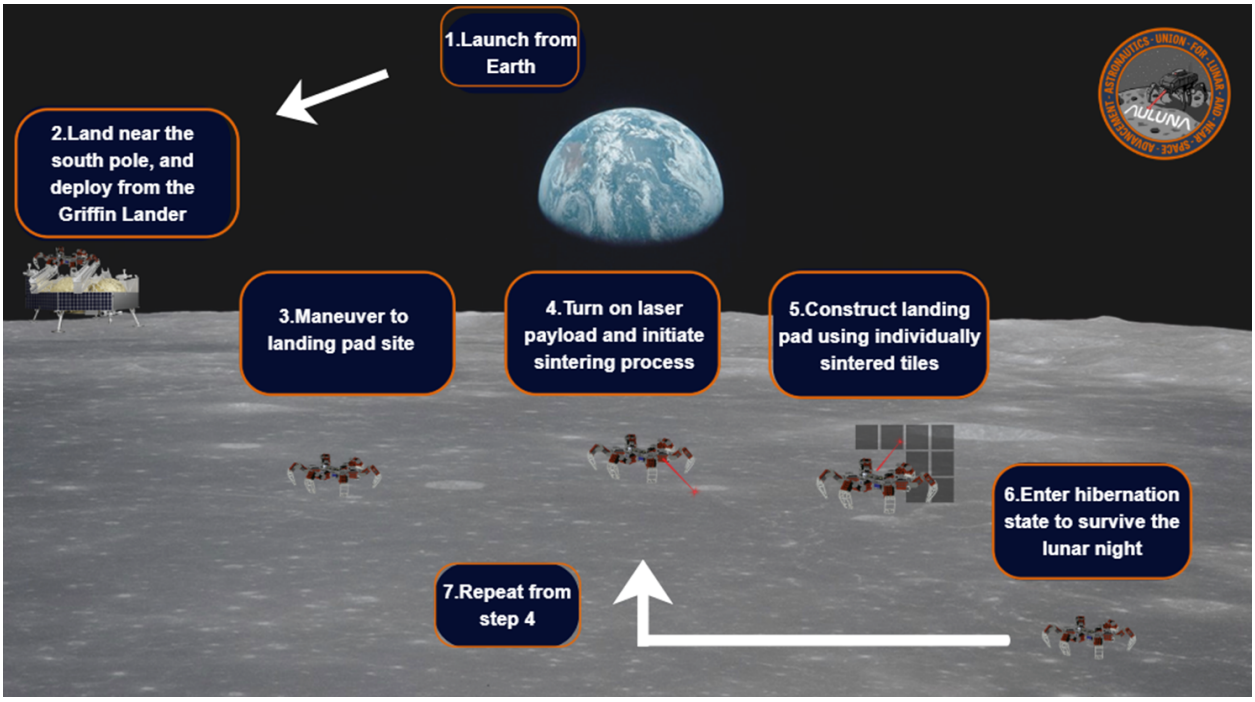

Fig. 1 Concept of Operations

III. The LSRH Design

A. Concept Overview

The LSRH mission seeks to accomplish two goals: constructing one LLP and demonstrating the capability of a hexapod mobility system on lunar terrain. The LSRH is designed first and foremost as a means by which an LLP can be constructed to facilitate future lunar operations. A high-level flowchart of the LSRH system and subsystems is depicted in Figure 2. The needs driving the development of each system include autonomous operation, thermal management, system power, communication, laser sintering operations, and hexapod mobility.

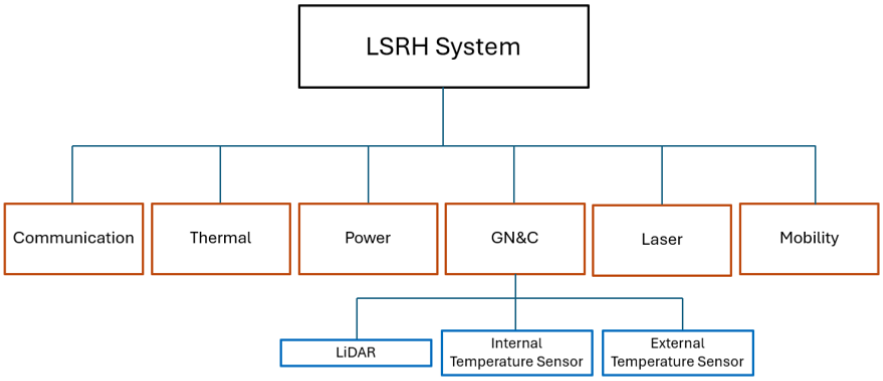

Fig. 2 LSRH System and its Subsystems

B. Requirements

Table 3 summarizes all requirements defined for the LSRH mission. The list of all requirements can be found in Appendix A. Requirements are grouped by functional, performance, constraint, and verification. Three tiers for the requirements are established, with Tier 2 and 3 requirements flowing down from the Tier 1 requirements. In Table 3, this tier enumeration is indicated by the number in the parenthesis after the requirement title. Requirements have been defined for the overall mission, payload, laser system, mobility system, guidance and navigation system, communication system, power system, thermal system, and mission safety. A visualization of the LSRH mission requirements hierarchy is depicted in Figure 3.

Table 3 Requirements by Type and Hierarchy

Functional	Performance	Constraint	Verification
R-MIS-010 (1)	R-MOB-020 (2)	R-MIS-030 (1)	R-MIS-040 (1)
R-MIS-020 (1)	R-MOB-030 (2)	R-LAD-010 (1)	R-MIS-050 (1)
R-LAD-020 (1)	R-MOB-060 (2)	R-MOB-050 (2)	R-MIS-060 (2)
R-PLD-010 (2)	R-LAS-020 (2)	R-COM-010 (2)	R-MIS-070 (1)
R-PLD-020 (2)	R-LAS-030 (2)	R-PWR-010 (2)	R-MOB-070 (2)
R-MOB-010 (2)	R-LAS-040 (2)	R-SAF-010 (1)	R-MIS-080 (1)
R-MOB-040 (2)	R-LAS-050 (2)	R-LAS-070 (2)	
R-LAS-010 (2)	R-LAS-060 (2)		
R-GNC-010 (2)	R-GNC-050 (3)		
R-GNC-020 (3)	R-THM-010 (2)		
R-GNC-030 (3)			
R-GNC-040 (3)			
R-GNC-060 (3)			
R-GNC-070 (3)			
R-SAF-020 (1)			

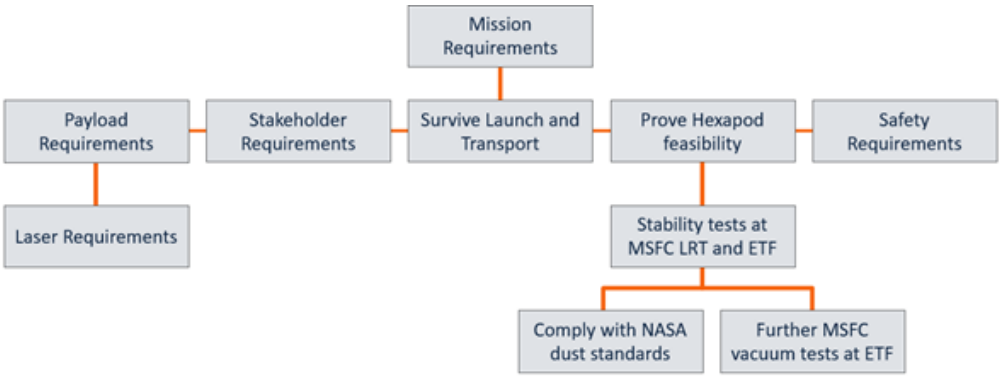

Fig. 3 Summary of LSRH Mission Requirements

C. Design

The LSRH is a 6-legged robotic hexapod with a rectangular body. The LSRH design is shown in Figure 4. The legs consist of 18 servos, each with two joints, connecting a femur and a tibia. A 6-DOF industrial robot arm is mounted as the payload on the top of the body section, featuring the fiber optic laser payload and a visual sensor suite. Dust covers and sealants are used to protect the joints, actuators, electronics, and other vital internal components. A tether boom is mounted on the rear of the hexapod and is used to connect to the Griffin Lander for power. LiDAR sensors, cameras, gyroscopes, accelerometers, GPS systems, thermal sensors, and other sensors are featured throughout the body segment internally and externally to allow for the collection of necessary telemetry, mission diagnostics, and autonomous operations data. Electrodynamic dust shields comprised of indium tin oxide electrodes will be used to protect sensor equipment from lunar regolith contamination [14]. The hexapod feet are a novel "snow shoe" design [15]. Each foot is split into two main parts: a spherical contact and a spring-activated extension mechanism that unfolds into an umbrella shape to provide a larger support area in response to sinking into regolith. The combination of these features will lead to needed stability on lunar terrain. Figure 5 presents a labeled diagram of key LSRH components.

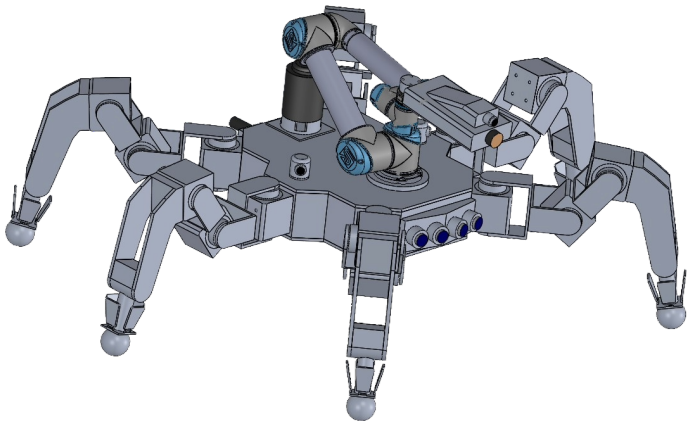

Fig. 4 LSRH Design

The materials used for the LSRH mission are selected for performance in extreme lunar conditions. The LSRH must be able to survive extreme temperatures, constant radiation, abrasive lunar regolith, and mechanical wear. Titanium and aluminum alloys will be used for the bulk of the structure, as these materials are well-suited for these conditions. Insulating materials, used to protect sensitive electronics and other equipment, will include Mylar multilayer insulation, aluminized kapton, and fiberglass cloths. Leg joints and bearings will need to withstand wear and corrosion. Therefore, a resilient material, such as AISI 440C stainless steel, will be used for these applications.

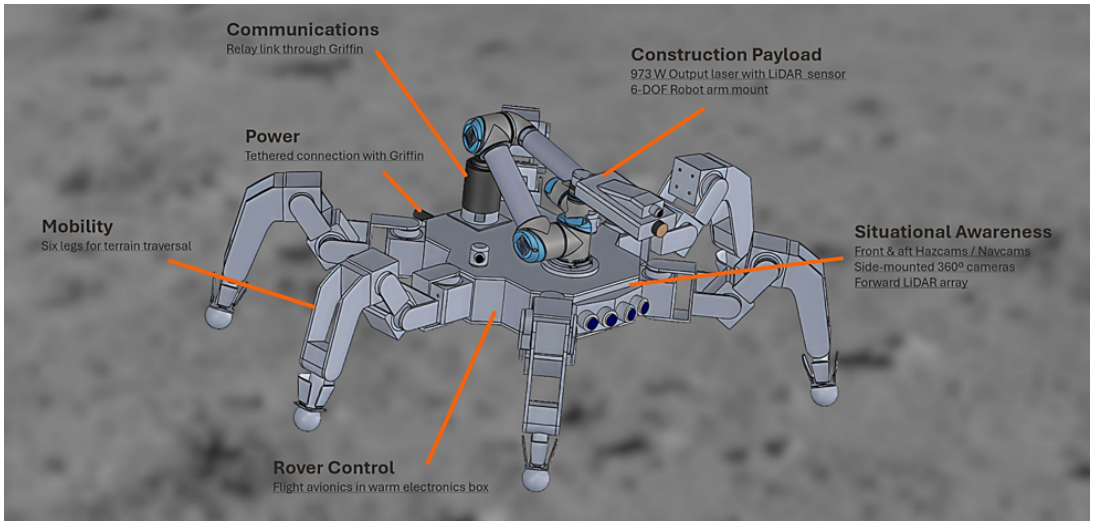

Fig. 5 LSRH Design with Components Labeled

The LSRH has 3 separate configurations over the mission duration: launch and delivery, standard, and hibernation. These configurations are shown in Figure 7. The launch and delivery configuration is necessary to meet the constraints of the Griffin lander. The LSRH will fold its two middle legs up on both sides of the body, becoming a quadruped. It will then dismount the Griffin down the delivery ramp while walking on these 4 legs. Figure 8 shows the launch and delivery configuration fitting within the Griffin lander volumetric constraints, which are described in a later section.

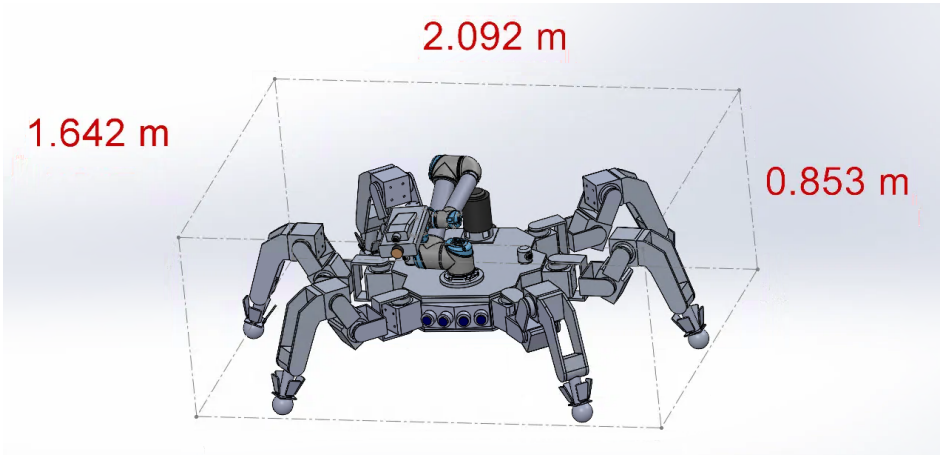

Fig. 6 LSRH Design with Dimensions, Standard Configuration

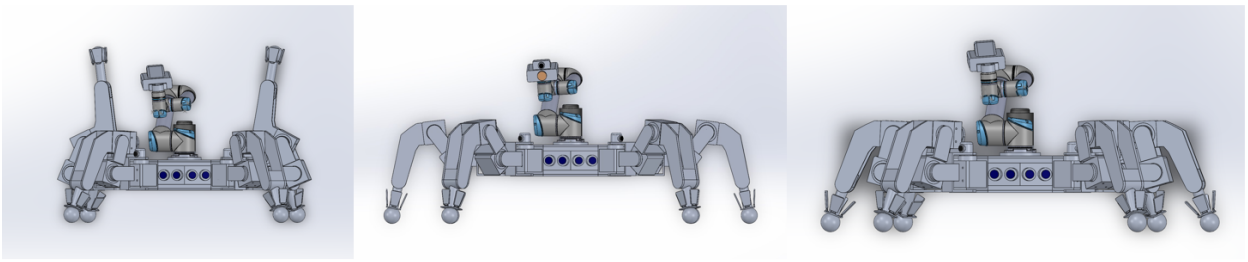

Fig. 7 LSRH Configurations (Left to Right: Launch and Delivery, Standard, and Hibernation)

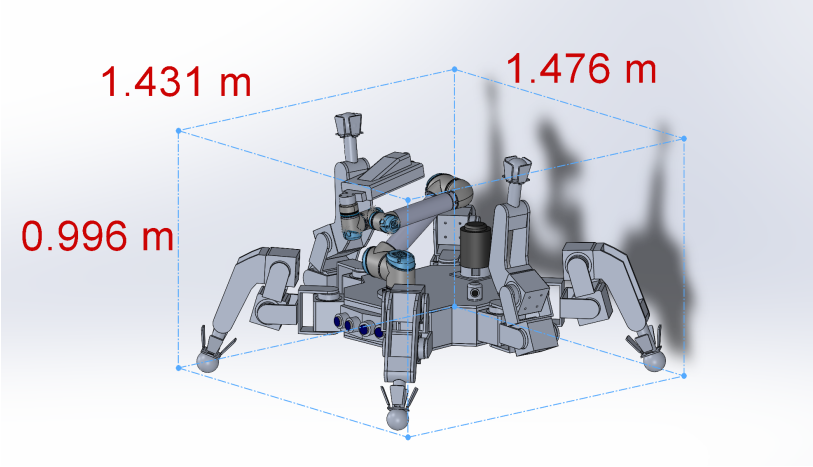

Fig. 8 Dimensions of the LSRH, Launch and Delivery (Quadruped) Configuration

1. Constraints and Design Choices

The LSRH mission operates under numerous constraints. The primary source of constraints is the delivery vehicle used for this mission: the Astrobotic Griffin Lander [16]. These constraints are summarized in Table 4. The relatively low mass allowed requires a design that optimizes structural integrity with low weight. The laser system must also be designed so as not to occupy too much mass or volume on the vehicle. The LSRH will fit inside the Griffin payload bay by folding its hexapod legs, showing a key attribute of the hexapod mobility system in meeting volume constraints. A depiction of the available payload volume dimensions is shown in Figure 9. The power provided by the Griffin is high, allowing laser sintering operations with a continuous source of power. Because of the abundant solar panels on the Griffin lander, the LSRH will utilize a tethered connection to the lander. Further discussion of this design choice is found in the Risk Assessment section. The Griffin communication system, which features adequate uplink and downlink capabilities for communicating with Earth, provides ample accommodation for the simple communication requirements of the LSRH.

Table 4 Griffin Lander Constraints

Constraint	Volume	Mass	Power Provided	Communication
Value	1.7m x 1.75m x 2.5m	200 kg	5 kWe	5G relay 60 Mbps

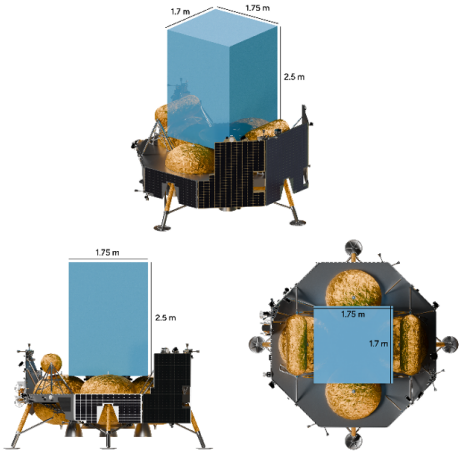

Fig. 9 Volumetric Constraints inside the Griffin Lander

Further constraints for the LSRH mission arise from the harsh lunar environment. The summary of lunar surface constraints can be found in Table 5. The topography of the lunar surface is dominated by craters and ejecta, producing localized steep slopes, terrain roughness, and obstacles that can destabilize rover platforms and landing vehicles. According to NASA's Lunar Surface Databook, the expected mean slopes of the south pole region range from $7° - 8°$. Maximum slopes range from $27° - 41°$ [17]. While the construction of the LLP in this mission is planned to occur on mostly flat terrain, the LSRH will be designed to maintain stability up to a slope angle of 30°, a margin that allows the platform to operate well within the expected average lunar surface conditions. This will require conservative path planning to avoid the most extreme slopes.

Table 5 Lunar Terrain Constraints (Key Quantities)

Constraint	Value
Mean south pole slope	7°–8° [17]
Max south pole slope	27°–41° [17]
LSRH slope stability requirement	30°
Equatorial daytime surface T (maximum)	387–397 K [18]
South pole surface T (minimum)	~ 60 K [19]
Typical lunar night duration	~ 15 days [20]
Min night duration (SP regions near Shackleton / Nobile Rim 2)	~ 43 hr [21]
Max tectonic moonquake magnitude (Richter)	~ 4.1 [22]

Obstacles, such as large rocks or boulders, are expected. Many of these obstacles are anticipated to be around the crater rims, which will constrain foot placement and allowable step height, potentially posing a risk of collision. LiDAR sensors on the rover will be used for surface mapping, allowing for paths to be created to avoid these obstacles. The hexapod configuration may also allow the rover to simply step over some rocks and smaller boulders, effectively neutralizing the risk of collision.

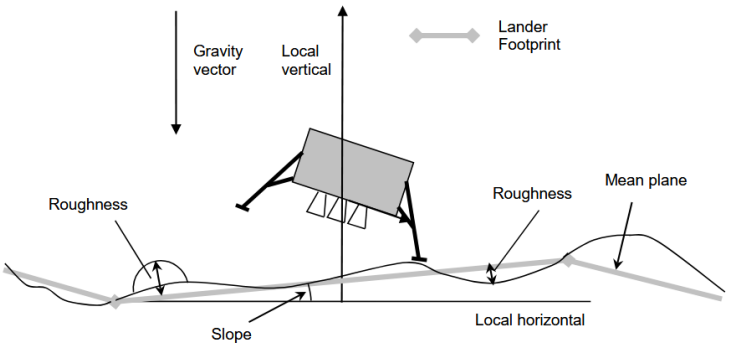

Fig. 10 A Depiction of Lunar Surface Hazards upon Landing [23]

The porosity and granularity of regolith also vary depending on the region of the lunar surface. Many of the considered landing sites for the Artemis program lie within the lunar highlands regions of the south pole [1]. With the LSRH mission aiming to operate within the bounds of Artemis IV, the prospective landing site will be Nobile Rim 2. This location is within the lunar highlands region and was found to be the optimal landing site out of the potential Artemis landing sites [24]. This landing site will have a similar regolith profile to that of the Apollo 14 and Apollo 16 missions, from which many samples were returned to Earth for study. Regolith in the highlands region is described as light and very loosely packed [25]. As demonstrated by landings during the Apollo missions, much of the regolith on the near-surface regions is extremely susceptible to creating large dust plumes, while density increases as depth increases [25]. It will be critical that the hexapod's leg design features wide feet so that the rover is capable of traversing the surface of the lunar highlands. The prototype hexapod will be tested at MSFC's Lunar Regolith Terrain (LRT),

which features JSC-1 Mare Regolith simulant [26]. Although the Mare regolith consists of rougher basaltic rocks, a demonstration of navigation in a relevant environment will still be extremely beneficial for proving the mission's feasibility.

Lunar regolith does not just pose a challenge to traversing the lunar surface. As previously mentioned, the lack of atmosphere and low gravity causes lunar regolith to float freely, often electrically charged. These floating particles could severely damage landing spacecraft and rovers on the surface; gears and other components in actuators, joints, electronics, and more are susceptible to this damage. To prevent dust damage, the LSRH will utilize dust mitigation strategies that have been demonstrated on previous and future NASA missions, such as VIPER and the Perseverance rover. Using a similar strategy to the VIPER rover, the LSRH will feature "socks," fabric seals that flex with the actuators and joints, preventing dust from getting in while not constricting motion [27]. Furthermore, the dust mitigation strategies will be informed by the standards outlined in NASA-STD-1008 [28].

Fig. 11 "Socks" Found on the VIPER Rover Preventing Dust Damage [27]

The most important constraint being considered for the mission is the rover's ability to survive lunar night conditions. Lunar weather consists of extreme heat and cold conditions. Daytime temperatures can reach a maximum of 387K to 397K at the equator, dropping to 95K before lunar dawn [18]. At the south pole, these temperatures can even reach as low as 60K [19]. A typical lunar day-night cycle will see 15 days of illumination followed by 15 days of darkness [20] [21]. However, in the south pole regions, illumination periods could reach beyond 15 days with subdivided illumination-darkness periods. NASA has found that regions around Shackleton Crater can have lunar nights that last as little as 43 hours [29]. As the mission is expected to utilize Nobile Rim 2 as the landing site, a lunar night of 43 hours will be assumed as the best-case scenario. During the night, the LSRH will utilize power from the Griffin Lander to power its heating systems while entering a hibernation state. This state will emulate that of the VIPER mission, which is also planned to utilize the Griffin Lander [30]. Constant power, stored at 8 kWhr, is expected to last Griffin over 100 hours during nighttime conditions, indicating the system will survive the expected duration of the lunar night and will be able to support the LSRH during rover hibernation status [16].

Other considerations regarding lunar weather include tectonic events induced by thermal shock at the day-night transition, dubbed "moonquakes." There are two sources of moonquakes. The first is major tectonic events occurring due to the Moon shrinking as its interior cools. The other is from the contraction and expansion occurring during the sudden extreme temperature transitions in the day-night cycle. The most extreme seismic events occur due to tectonic activity deep within the Moon's interior, which can reach up to 4.1 on the Richter scale and last up to 10 minutes in duration [22]. These tectonic events could also create instability for the lander and rover, potentially damaging the LLP as it is being constructed. In the future, major seismic events could even damage or destroy established lunar infrastructure. Although there is a great danger posed in the long-term, for the short-term goals of the LSRH mission, the expected main source of moonquakes will be from thermal shocks. These seismic events are small in magnitude and are regarded as unlikely to cause damage to a lunar habitat [31]. However, should the mission encounter a major tectonic event, the inherent stability of the hexapod will be leveraged to maintain the payload's safety. There remains an inherent risk of damage to the LLP and Griffin Lander. Once again, conservative mission planning is paramount to avoid potentially severe consequences from significant seismic events.

2. Selected Trade Study

Several trade studies were conducted during the conceptual design of the LSRH mission. This section presents the rationale and results of one trade study: the laser sintering device. Figure 12 presents the figures of merit for the laser

sintering device trade study. The two highest weighted items are the sinter efficiency and sinter quality. The efficiency merit considers how efficiently the regolith is sintered. The power consumption of the laser relative to the power density output onto a surface is the qualitative way in which laser sintering devices are compared. The quality merit considers whether the regolith will be sintered properly by the laser or not. In other words, the amount and severity of defects in the sintered product is used for comparison of methods. The two other figures of merit, weighed equal to one another, are the fragility of the device and space needed for the device. The fragility is important because a launch from Earth will subject the entire LSRH to heavy vibrations. The mechanical weaknesses inherent to the device are considered in this merit. Finally, the space necessary for the device is important because of the Griffin Lander volumetric constraints. Space will be at a premium on the LSRH body, so minimizing the space taken up by the laser device is important.

Figure of Merit	Weight(%)	CO2 Laser	Fiber Optic Laser	Diode Laser
Sinter Efficiency	0.35	0	0	0
Sinter Quality	0.35	0	0	0
Fragility	0.15	0	0	0
Space Allocated	0.15	0	0	0
	1	0	0	0

Fig. 12 Laser Sintering Device Trade Study Figures of Merit

Figure 13 shows the completed trade study for the laser sintering device. The fiber optic laser, being the most efficient and well-performing method, was found to be the optimal choice for the LSRH mission. The space needed for this was also found to be the lowest. Although a fiber optic laser is not the most resilient structure, its performance across the other figures of merit led to it being chosen for the LSRH mission. Key features of the fiber optic laser method include high efficiency, medium power consumption, flexible fiber cable and interchangeable frame, and relatively low fragility and bulkiness. Comparison information for the trade study was obtained from Ref. [5] and Ref. [32].

Figure of Merit	Weight(%)	CO2 Laser	Fiber Optic Laser	Diode Laser
Sinter Efficiency	0.35	4	5	3
Sinter Quality	0.35	4	5	3
Fragility	0.15	2	4	5
Space Allocated	0.15	2	5	5
	1	3.3	4.8	3.7

Fig. 13 Completed Laser Sintering Device Trade Study

3. Power Availability Calculation

To determine how much power can be allotted to the laser sintering system, a preliminary power budget was developed. A key assumption used in this analysis was that the planned power will be 50% above the estimated needed power. This will account for changes moving forward in the design, fluctuations in available power from the Griffin Lander, and power needed to regulate LSRH temperature. Table 6 shows the values used in this analysis. These values were taken mainly from systems available in the literature [30] [33]. As a result of this power budget, the best-case and worst-case laser system available powers of 2833 Watts and 2633 Watts were determined using the available Griffin power of 5 kW.

Table 6 Preliminary Power Budget Before Laser Payload Considered

Consumption	Mobility (W)	Systems (W)	Total Power (W)	Total Power + 50% (W)	Power Left (W)
Low	300	200	500	750	2633
Medium	300	300	600	900	2733
High	300	400	700	1050	2833

4. Mass Budget Calculation

The total mass allowed as a payload on the Griffin Lander is 200 kg. To understand how that total mass should be allocated to the subsystems, a preliminary mass budget was compiled. This preliminary budget was based on a small-scale prototype with a twenty-five percent contingency built in. This analysis, shown in Table 4, leads to a preliminary allocation of the mass for each subsystem on the flight model. The payload on the prototype is not as high-fidelity as the anticipated payload on the flight model design. Because of this, twenty-percent of the total mass will be allocated to the payload for the flight model design. This will be taken from the allocated structure mass, as it is not expected that the flight model will require a 154 kg structure.

Table 7 Preliminary Mass Budget of Prototype and Flight Model

Prototype Total Mass	2.268 kg			
Total Flight Mass	178.503 kg **(200 kg allowed)**			
Subsystem	**Structure**	**Sensors and Controls**	**Electrical and Computer**	**Payload**
Prototype Subsystem Mass	77% (1.746 kg)	13% (0.294 kg)	5% (0.113 kg)	4.9% (0.131 kg)
Max Subsystem Allocated Flight Mass	154.08 kg	27.06 kg	11.93 kg	9.881 kg

5. Laser Operations

The laser system featured as the payload for the LSRH was developed to tackle the challenge of ISRU manufacturing of an LLP. The development of laser sintering technology remains a significant challenge, yet it is crucial to the mission objectives and future utilization of the lunar surface.

To construct lunar infrastructure, the laser must be able to heat the surface to the melting temperature of lunar regolith, which peaks at 1150 degrees Celsius [34], then let the surface cool into a solid glassy structure. Volumetric energy densities between 10 and 16 J/mm^3 [34] were found to be sufficient to melt regolith. An analysis was conducted to determine the time it would take to construct a hexagonal tile with a width of one meter. Hexagonal tiles were chosen to modularity approximate a circular launchpad while simplifying laser fabrication. To perform this analysis, TruFiber P Compact fiber optic lasers [35] were paired with optical lenses suitable for laser applications [36]. This was done to serve as a baseline estimation of how long and how much energy it will take to construct a singular tile by calculating the best- and worst-case scenarios and averaging them. Both the fiber optic lasers and optical lenses were chosen to meet mission requirements to maximize compactness of the LSRH and minimize the time needed to complete a tile. This was done particularly by choosing a reasonable focal length of 500mm for the focusing optic and a small collimator focal length of 12.7mm to maximize the spot diameter. The spot diameter was then used as the hatch spacing, which assumes the laser perfectly traces the object with no overlapping. To obtain the surface energy density, it was assumed that a 2mm melt depth would be used on the lunar surface. The best- and worst-case scenarios were calculated by using the upper and lower limits of the volumetric energy densities. Likewise, the upper and lower bounds for power efficiency are 30 and 40 percent for fiber optic lasers.

The results of the analysis show that lasers at and above 500 Watts of output power allow for the completion of a tile in less than 12 hours. A tile can be completed in less than 3 hours as the output power increases beyond 1500 Watts, according to the averaged results in Table 10. The lower and upper bounds for energy required to finish one tile are 9.02 and 19.25 kilowatt-hours, respectively, with an average of 14.13 kilowatt-hours. This large expenditure of energy could present operational concerns with the 8-kilowatt-hour energy storage limit inside the Griffin lander, reducing lunar night capabilities. To construct an 18-meter diameter launchpad, 245 hexagons are needed as seen in Fig. 15. With an output power greater than 1500 watts, it is theoretically possible to complete a launchpad within 30 days. However, this is unlikely since continuous operation of the hexapod could result in damage and lunar night energy consumption must be kept at a minimum, resulting in a longer time for completion. From the preliminary power budget, a maximum of 2633 Watts and 2833 Watts can be allocated to the laser sintering operation in the worst-case and best-case, respectively. The average between these values, 2733 Watts, was chosen for the analysis. This corresponds to an output power of 937 Watts. Table 11 summarizes the results for this output power with a launchpad completion time of 51 days.

$$d_{\text{spot}} = \frac{4\lambda f M^2}{\pi D_{\text{beam}}} \tag{1}$$

Equation (1) represents the spot diameter, this can be found at Eq. 2.33 in [37]. The values for wavelength and beam quality factor were taken from the specifications of the laser, the focal length of the focusing optic was maximized, assuming that there is at least 500mm between the laser payload and the lunar surface. The beam diameter before reaching the focusing optic was minimized to ensure a large spot diameter. A large spot diameter is preferred to ensure a reduction in processing time.

$$D_{\text{beam}} = 2 f_c \theta \tag{2}$$

Equation (2) shows the beam diameter calculation which can be found in [38]. The numerical aperture is very small for fiber optic lasers, usually around the 0.1 range, since there is a narrow angle of light leaving the laser. Additionally, the focus length for the collimating lens was chosen to be small to reduce the beam diameter so that more light will scatter.

$$v = \frac{P}{E_{\text{surface}}\, d_{\text{spot}}} \tag{3}$$

Scanning speed is calculated by dividing the power of the laser by surface energy density and spot diameter, as shown in Eq. (3), this relationship can be found at Eq. 1 in [39]. The surface energy density was found by multiplying the volumetric energy density by the 2mm melt depth discussed earlier.

$$t = \frac{A_{\text{hex}}}{v\, h} \tag{4}$$

The relationship in Eq. (4) was rearranged from the areal rate of a laser being scanned, speed times hatch spacing ($A/t = v * h$). The completion time for a selected area can be found through this modified version of the equation. Hexagon tiles were chosen to construct the launch pad. A width of 1 meter was chosen as a base estimate for the completion of large-scale objects using the fiber optic laser payload of the selected parameters. The area of a hexagon is given in Eq.(5).

$$A_{\text{hex}} = \left(\frac{3\sqrt{3}}{2}\right) \cdot a^2 \tag{5}$$

In calculating the area of a regular hexagon, the side length a was chosen to be 500mm for the analysis.

Table 8 Worst-Case Time and Energy Results

P_{out} (W)	250	500	750	1000	1250	1500	1750	2000	2250	2500	2750	3000
P_{in} (W)	833	1667	2500	3333	4167	5000	5833	6667	7500	8333	9167	10000
Tile Completion Time (hrs)	23.09	11.55	7.70	5.77	4.62	3.85	3.30	2.89	2.57	2.31	2.10	1.92
Launchpad Completion Time (Earth days)	235.8	117.9	78.6	58.9	47.2	39.3	33.7	29.5	26.2	23.6	21.4	19.6
Energy Needed to Complete a Tile (kWh)	19.25	19.25	19.25	19.25	19.25	19.25	19.25	19.25	19.25	19.25	19.25	19.25
Total Energy Consumption (kWh)	4715	4715	4715	4715	4715	4715	4715	4715	4715	4715	4715	4715

Table 9 Best-Case Time and Energy Results

P_{out} (W)	250	500	750	1000	1250	1500	1750	2000	2250	2500	2750	3000
P_{in} (W)	625	1250	1875	2500	3125	3750	4375	5000	5625	6250	6875	7500
Tile Completion Time (hrs)	14.43	7.22	4.81	3.61	2.89	2.41	2.06	1.80	1.60	1.44	1.31	1.20
Launchpad Completion Time (Earth days)	147.34	73.67	49.11	36.84	29.47	24.56	21.05	18.42	16.37	14.73	13.39	12.28
Energy Needed to Complete a Tile (kWh)	9.02	9.02	9.02	9.02	9.02	9.02	9.02	9.02	9.02	9.02	9.02	9.02
Total Energy Consumption (kWh)	2210	2210	2210	2210	2210	2210	2210	2210	2210	2210	2210	2210

Table 10 Averaged Time and Energy Results

P_{out} (W)	250	500	750	1000	1250	1500	1750	2000	2250	2500	2750	3000
P_{in} (W)	729	1458	2188	2917	3646	4375	5104	5833	6563	7292	8021	8750
Tile Completion Time (hrs)	18.76	9.38	6.25	4.69	3.75	3.13	2.68	2.35	2.08	1.88	1.71	1.56
Launchpad Completion Time (Earth days)	191.5	95.8	63.8	47.9	38.3	31.9	27.4	23.9	21.3	19.2	17.4	16.0
Energy Needed to Complete a Tile (kWh)	14.13	14.13	14.13	14.13	14.13	14.13	14.13	14.13	14.13	14.13	14.13	14.13
Total Energy Consumption (kWh)	3352	3352	3352	3352	3352	3352	3352	3352	3352	3352	3352	3352

Table 11 Averaged Time and Energy Results for Power Balance

P_{out} (W)	937
P_{in} (W)	2733
Time to Complete a Tile (hrs)	5.01
Launchpad Completion Time (Earth days)	51.1
Energy to Complete a Tile (kWh)	14.13
Total Energy Consumption (kWh)	3352

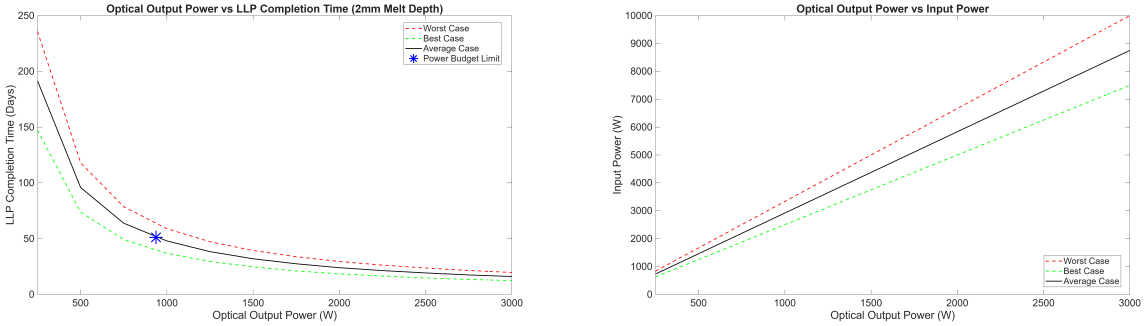

(a) Output Power vs LLP Completion Time **(b) Optical Output Power vs Input Power**

Fig. 14 Laser Performance Calculation Plots

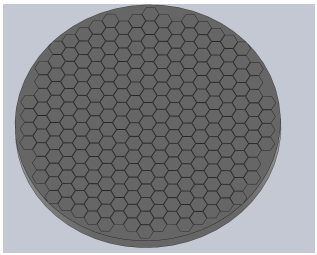

Fig. 15 Honeycomb Patterned Launchpad

6. Hexapod Mobility System

The key unique aspect of the LSRH system is its 6-legged hexapod configuration. The hexapod configuration will ensure the system's terrain adaptability, precise foot placement, and static stability during sintering operations on the uneven lunar surface. This novel mobility system could one day be used to propel exploration vehicles on future lunar or Martian missions, perhaps even propelling drones as part of swarm-based robotics plans [40].

Key mission requirements directly inform the hexapod's configuration. A list of the requirements is contained in Addendum A. Because the mobility system is expected to be advantageous for navigating the harsh surface, it is required to maintain static stability on a slope of up to 30°. The control system for prototype testing will also be required to have a latency of less than 10 ms between inputs and outputs. However, the actual rover that will be deployed is expected to act fully autonomously while still allowing direct human intervention. To allow the system to maintain power requirements for the other subsystems, the mobility system is required to maintain a Cost of Transport (CoT) below 4.0. These requirements are critical not only for traversing the rough, sloped terrain near the lunar south pole but also for maintaining the stability and system requirements to enable laser sintering operations. Much of the prototype's testing will be conducted at MSFC's LRT, allowing for direct verification of system requirements.

To validate the hexapod design, several analyses have been performed. First, CoT calculations inform the system requirements. Next, inverse kinematics (IK) models enable code development for the hexapod's gait to further inform power analysis. Computer-aided design (CAD) models were developed, allowing for the determination of the prototype's design budget and mass. The mass will also allow for more analyses of the CoT for the prototype to be performed. Based on all of these parameters, a preliminary energy budget can be derived.

Unlike a wheeled rover, a hexapod depends on IK to allow any type of movement. In classical physics with movement (kinematics), angles between an object and its start and ending locations are known. In the case of the hexapod, the legs will have to change angles depending on how far a given step distance is, resulting in an unknown angle for the leg. This form of kinematics, in which the angle is unknown, is the basis of IK.

IK problems can be solved with different methods, but the most common is Euler angle parameterization. Euler angles are set as three angles, denoted as ϕ, θ, and ψ. These angles rotate along the x-axis (roll), y-axis (pitch), and z-axis (yaw), respectively. With these rotation angles, in addition to translation along an axis, there are six total potential degrees of freedom [41]. For the LSRH, there is a total of twenty-four degrees of freedom for the mobility system. Inclusion of the arm brings the total to thirty degrees of freedom, as the arm itself has six degrees of freedom. The LSRH is split between three degrees of freedom for each leg, accounting for the hip, femur, and tibia. Rotations between all six legs will result in the translation of the robot itself; rather than a singular component that translates, the robot will move forward along an axis from combinations of rotations in each leg.

Figure 16a displays how the joints in each leg have their own coordinate frames. A triangle, alternating between obtuse and acute as rotations about the "knee" occur, can be created by connecting the origin of each frame. Using that triangle and the law of cosines and sines, angular rotation rates can be determined. The leg itself is highlighted in Figure 16b with the orientation of the knee joint, hip area, and foot. A right triangle created by the foot and the z-axis and the distance from the hip to the foot is displayed. The angles that create both the right triangle and the other triangles are the angles used within the trigonometric calculations. Rotation rates give the prescribed angle needed to traverse a given distance. These rates are also ideal when writing code for a controller because the hexapod will not become inundated with commands and can instead freely walk at different speeds and directions.

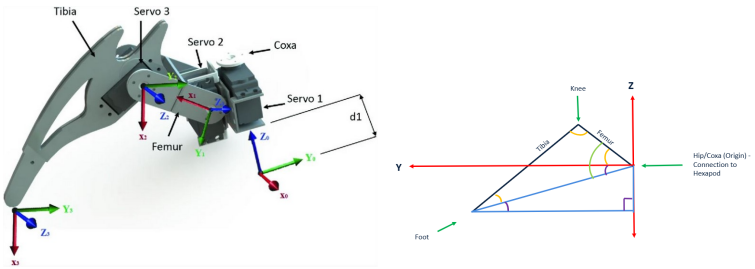

(a) Example Hexapod Leg [42] **(b) Hexapod Leg Diagram with Plot**

Fig. 16 Hexapod Leg Example and Diagram

While the prototype of the LSRH will be remotely controlled, the goal of the flight model is autonomous operation. Through autonomous control, developments of machine learning to help train the rover's controller on what actions to

complete depending on certain obstacles could be beneficial for the cost of transport as well as to bridge technology gaps. NASA has investigated applications of machine learning in robots, creating the Regolith Advanced Surface Systems Operations Robot, and testing has shown positive results [43].

At this stage, several of the requirements have been met in the analysis, notably the power requirement. The mobility requirements are currently pending experimental verification, as AULUNA plans to test the prototype at MSFC's LRT [26]. These tests will enable demonstration of the prototype in a relevant environment, providing a useful experiment to understand advanced robotic locomotion for lunar applications.

D. Risk Assessment

As part of the mission design process, a risk assessment was conducted for the LSRH. A visual depiction of all risks is presented in Figure 17. This section will focus on several identified critical risks and the proposed mitigation strategies for each one. Risks are categorized based on likelihood, severity of consequence, and type. The likelihood and severity were given numerical values that were then multiplied to obtain a final risk score. This score conveys the relative importance of each risk, and the risks with the highest scores are the ones discussed in this section.

One of the most pressing risks is the potential misalignment of the laser optic system. Alignment of the laser system is critical for system performance, as laser performance is directly dependent on the angle of incidence, and the LSRH programming will be designed for a specific design value. Misalignment is most likely to occur during launch and transport of the LSRH because of vibratory loads. This is because fiber optic lasers tend to be fragile and sensitive to external loads. Misalignment could also occur during the manufacturing process. As a result of these possibilities, the mitigation strategy focuses primarily on Earth-based testing and evaluation. Extensive vibration testing must be performed to ensure the laser can withstand a load greater than that of launch. Quality testing must also be performed upon receipt from the manufacturer to ensure the laser performs as expected. If the laser fails these tests, the design must be enhanced to pass mission requirements.

Another key risk is the potential for the regolith on the lunar surface to differ meaningfully from the regolith simulants available on Earth. This would result in sintered properties that differ from the expected values, as the type and quality of sintered material greatly impact the final product. This is an environmental risk, so the mitigation plan focuses on adapting to several possibilities. The LSRH design must conform to a range of expected values for material properties rather than specific individual values. Research must be performed to quantify these ranges, which will then be used to constrain system performance.

The final key risk discussed here is the potential for the LSRH to trip on or otherwise become entangled in the tether power cable. This could result in mission failure because the LSRH has no gripping arm available to assist in freeing itself, and mobility is critical for the mission. To mitigate this risk, several solutions are proposed. First, a boom will be constructed to extend the tethered connection away from the LSRH and its legs. Second, a light amount of tension will be applied to the cable connecting the LSRH and the Griffin lunar lander. Finally, AI tools will be employed to train the LSRH mobility system on Earth in freeing itself from several potential entanglement scenarios. This will hopefully lead to the LSRH gaining the ability to free itself if all other mitigation strategies fail.

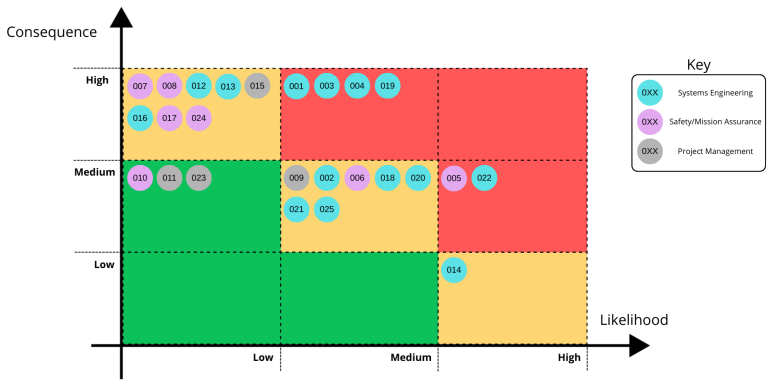

Fig. 17 Visual Depiction of Risk Assessment

IV. LSRH Prototype

A prototype was constructed to advance the LSRH design. The focus of prototype development was to prove the feasibility and potential of the hexapod mobility system. Extensive work was performed to create a controls system. Figure 18 shows a labeled CAD prototype model. The specifications of all electronic components placed on the prototype are listed. The prototype is controlled by an Arduino Mega 2560, utilizing an ESP32 as a Bluetooth link with a generic gaming controller for user control. Figure 19 shows the completed prototype. The structure was created with 3D printed PLA material. Testing was done to refine the controls system. The prototype was tested on flat terrain and sandy terrain, resulting in successful walking tests. A total of 3 walking gaits were developed: a standard gait, a high step standard gait, and a crab walk gait. The standard gait was based on a tripod gait, which provides stability and lower power usage [10]. The crab walk gait displayed the ability for the prototype to traverse horizontally, with no need for turning. Further refinement is ongoing for increased stability and maneuverability demonstrations.

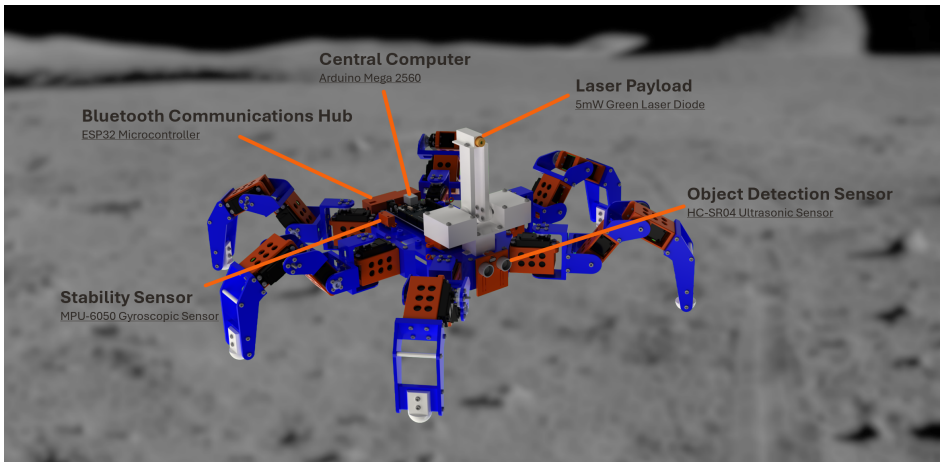

Fig. 18 Labeled Prototype CAD

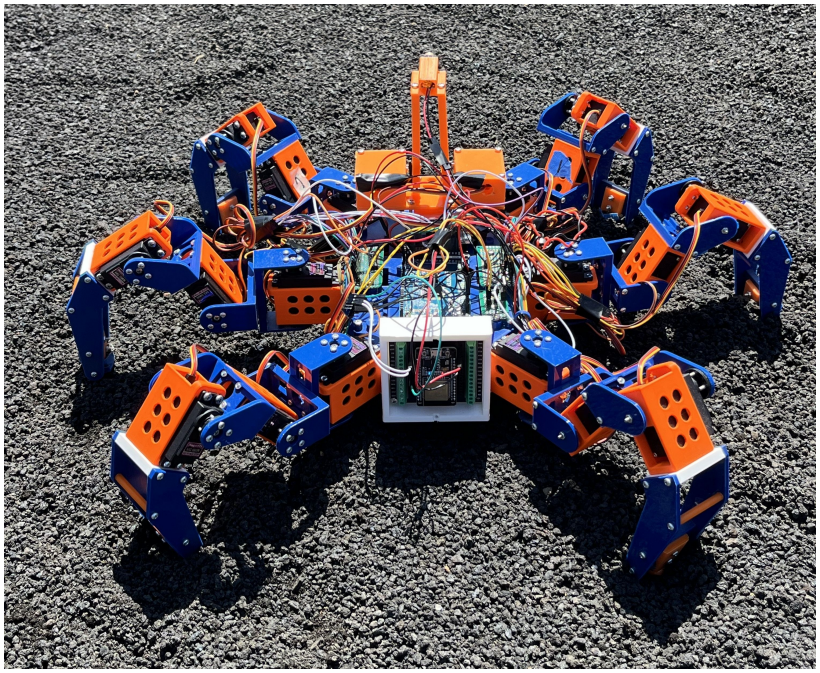

Fig. 19 Constructed Prototype

V. Conclusion and Future Work

The LSRH is a proposed mission to the lunar surface to construct one launch and landing pad that will support the NASA Moon to Mars Architecture. The LLP will serve as a key dust mitigation method as well as a platform for stability upon landing. Construction of this pad will be achieved via a laser sintering device attached to a biomimetic hexapod mobility system. The first main objective of this mission is to construct an 18-meter-diameter landing pad sufficient to support a medium-sized lunar lander. The next main objective is to prove the utility of the hexapod mobility system during a mission with relatively simple mobility requirements. Proving this mobility system is a crucial step towards designing rovers capable of traversing difficult terrain, which is the logical next step of lunar and Martian exploration and construction.

This mission is heavily constrained based on the planned delivery of the LSRH on board the Griffin lander. Restrictions on mass and size lead to a unique design that heavily utilizes the Griffin lander itself. The LSRH will be attached to the Griffin lander via a tethered power cable that will allow the rover to continuously utilize the large power output from the Griffin's large solar arrays. Additionally, all communications to Earth will be routed through the Griffin, which features adequate uplink and downlink capabilities for the mission. Current laser technology also constrains the mission to a slow construction process that will span multiple lunar days. As a result, much attention was devoted to surviving the lunar night during the design process. This issue is somewhat mitigated by the proposed mission location. Because the rover will be sent near the south pole region of the Moon, the day will be lengthened and the night shortened. The mission itself, provided only one LSRH rover is delivered to the Moon, will nevertheless result in just one landing pad, given these challenges.

The biggest lesson learned during this design process is that current laser systems are not adequate to construct an entire LLP in just one lunar day. Considerable effort must therefore be invested in designing an incremental construction process and in surviving the lunar night. Another lesson learned is just how hostile the lunar night is. The rapid cooling of any rover on the lunar surface will result in large thermal shock, which must be accounted for in the design process. An additional lesson is that the potential improvements in the design must be quantified to strengthen the argument for the design. Showing that a specific increase in performance may be achieved given a specific increase in, for example, power will not only convey understanding but also show a path for potential results from future research and development efforts.

Future work will focus on further quantifying laser system performance after a planned research and development phase. If this mission were to proceed, this phase would focus on improving laser performance at lower powers. This would result in a shorter time to mission completion. Additionally, a prototype is currently under development to show the feasibility of a hexapod mobility system in handling lunar-like terrain and maintaining stability for the laser system. Finally, more detailed work concerning the power system, local communication system, and controls system is planned.

VI. Acknowledgments

The AULUNA team thanks Dr. Davide Guzzetti and Jeremiah Tyrrell of Auburn University and Matt Anderson of Aerospace Corporation for their guidance on this work.

References

[1] NASA, "Artemis," NASA, Feb. 2026. URL `https://www.nasa.gov/humans-in-space/artemis/`, accessed April 3, 2026.

[2] Firefly Aerospace, "Blue Ghost," Firefly Aerospace, Oct. 2025. URL `https://fireflyspace.com/blue-ghost/`, accessed Oct. 6, 2025.

[3] Amos, J., "Intuitive Machines: Odysseus Moon Lander 'Tipped over on Touchdown'," BBC News, Feb. 2024. URL `https://www.bbc.com/news/science-environment-68388695`, published Feb. 23, 2024.

[4] Gelino, N. J., Mueller, R. P., Moses, R. W., Mantovani, J. G., Metzger, P. T., Buckles, B. C., and Sibille, L., "Off Earth Landing and Launch Pad Construction—A Critical Technology for Establishing a Long-Term Presence on Extraterrestrial Surfaces," *Earth and Space 2021*, American Society of Civil Engineers (ASCE), Apr. 2021, pp. 855–869. https://doi.org/10.1061/9780784483374.079.

[5] Ginés-Palomares, J.-C., Fateri, M., Kalhöfer, E., Schubert, T., Meyer, L., Kolsch, N., Lipińska, M. B., Davenport, R., Imhof, B., Waclavicek, R., Sperl, M., Makaya, A., and Günster, J., "Laser Melting Manufacturing of Large Elements of Lunar Regolith Simulant for Paving on the Moon," Scientific Reports, Oct. 2023. https://doi.org/10.1038/s41598-023-42008-1.

[6] Linke, S., Voß, A., Ernst, M., Taschner, P. A., Baasch, J., Stapperfend, S., Gerdes, N., Koch, J., Weßels, P., Neumann, J., Overmeyer, L., and Stoll, E., "Two-Dimensional Laser Melting of Lunar Regolith Simulant Using the MOONRISE Payload on a Mobile Manipulator," National Library of Medicine, Jun. 2022. https://doi.org/10.1089/3dp.2020.0323.

[7] Shake, P., "Additive Manufacturing Process Development DOE for NASA HR-1 using Laser Blown Powder Directed Energy Deposition ," NASA, Sept. 2023. URL https://ntrs.nasa.gov/citations/20230013640, accessed Feb. 19, 2026.

[8] NASA, "Space Technology Mission Directorate," NASA, Jan. 2026. URL https://www.nasa.gov/space-technology-mission-directorate/, accessed Jan. 12, 2026.

[9] Roditis, I., Nitsos, T., Porichis, A., and Panagiotis, "Maintaining Static Stability and Continuous Motion in Rough Terrain Hexapod Locomotion without Terrain Mapping," , August 2016. IEEE Conference Publication, https://doi.org/10.1109/MED.2016.7536027.

[10] Guo, Y.-Q., Luo, W.-H., Xu, Z.-D., Shu, B.-M., and Yang, D.-K., "Research on the Design and Gait Planning of a Hexapod Robot Based on Improved Triangular Gait for Lunar Exploration," *Applied Sciences*, Vol. 14, No. 1, 2024, p. 260. https://doi.org/10.3390/app14010260.

[11] Z.Y. Wang and X.-L. Ding and A. Rovetta, "Analysis of Typical Locomotion of a Symmetric Hexapod Robot ," ResearchGate, Nov. 2009. URL https://www.researchgate.net/publication/221907923_Locomotion_Analysis_of_Hexapod_Robot, accessed Feb. 19, 2026.

[12] Mount, E., Hollister, M., McNichol, C., Dyke, S. J., Ramirez, J. A., Sharma, A., and Bobet, A., "Lunar Landing and Launching Pad Design Considerations Using ISRU Materials," *Acta Astronautica*, Vol. 240, 2026, pp. 165–182. https://doi.org/10.1016/j.actaastro.2025.11.071.

[13] Blue Origin, "Blue Moon," Blue Origin, 2026. URL https://www.blueorigin.com/blue-moon, accessed Feb. 25, 2026.

[14] Buhler, C., Johansen, M., Dupuis, M., Phillips, J., Malissa, J., Wang, J., and Calle, C., "Current State of the Electrodynamic Dust Shield for Mitigation," 2020. URL https://ntrs.nasa.gov/citations/20200000920, NASA Technical Reports Server (NTRS), Document ID: 20200000920.

[15] Shu, B.-M., Guo, Y.-Q., Luo, W.-H., Xu, Z.-D., and Xu, Q., "Structure and Gait Design of a Lunar Exploration Hexapod Robot Based on Central Pattern Generator Model," *Actuators*, Vol. 13, No. 2, 2024, p. 79. https://doi.org/10.3390/act13020079.

[16] Astrobotic Technology, "Astrobotic Griffin Lander," Astrobotic Technology, Jul. 2023. URL https://www.astrobotic.com/wp-content/uploads/2022/01/PUGLanders_011222.pdf, accessed Jul. 6, 2023.

[17] Dishongh, L., "Lunar Surface Data Book," *Artemis Campaign Development (ACD) Document ACD-50044, Revision A*, May 2023. URL https://ntrs.nasa.gov/api/citations/20230007818/downloads/ACD-50044%20Lunar%20Surface%20Data%20Book%20Rev%20A.pdf, NASA Technical Reports Server (NTRS) Document ID: 20230007818; Effective date: May 25, 2023.

[18] Williams, J.-P., Paige, D. A., Greenhagen, B. T., and Sefton-Nash, E., "The global surface temperatures of the Moon as measured by the Diviner Lunar Radiometer Experiment," *Icarus*, Vol. 283, Feb. 2017, pp. 300–325. https://doi.org/10.1016/j.icarus.2016.08.012.

[19] Suggs, R., "What's the Weather Like on the Moon?" Presentation, Von Braun Astronomical Society (VBAS) Monthly Meeting, Huntsville, AL, United States, Mar. 2025. URL https://ntrs.nasa.gov/api/citations/20250003150/downloads/Weather%20on%20the%20Moon%20Suggs%20MSFC_LP10.pdf, NASA Technical Reports Server (NTRS) Document ID: 20250003150; meeting date: Apr. 18, 2025; acquisition source: Marshall Space Flight Center.

[20] Fincannon, J., "Lunar South Pole Illumination: Review, Reassessment, and Power System Implications," *NASA/TM–2007-215025 (AIAA Paper 2007–4700)*, Nov. 2007. https://doi.org/10.2514/6.2007-4700, NASA NTRS Document ID: 20070034951; Presented at the Fifth International Energy Conversion Engineering Conference and Exhibit (IECEC), St. Louis, MO, June 25–28, 2007.

[21] Speyerer, E. J., and Robinson, M. S., "Persistently Illuminated Regions at the Lunar Poles: Ideal Sites for Future Exploration," *Icarus*, Vol. 222, No. 1, Jan. 2013, pp. 122–136. https://doi.org/10.1016/j.icarus.2012.10.010.

[22] Ruiz, S., Cruz, A., Gomez, D., Dyke, S. J., and Ramirez, J., "Preliminary Approach to Assess the Seismic Hazard on a Lunar Site," *Icarus*, Vol. 383, Sept. 2022. https://doi.org/10.1016/j.icarus.2022.115056, NASA Technical Reports Server (NTRS) Document ID: 20240009464.

[23] Rosa, D. D., Bussey, B., Cahill, J. T., Lutz, T., Crawford, I. A., Hackwill, T., van Gasselt, S., Neukum, G., Witte, L., McGovern, A., Grindrod, P. M., and Carpenter, J. D., "Characterisation of potential landing sites for the European Space Agency's Lunar Lander Project," *Planetary and Space Science*, Vol. 74, Aug. 2012, pp. 224–246. https://doi.org/10.1016/j.pss.2012.08.002.

[24] Peña-Asensio, E., Álvaro Steve Neira-Acosta, and Sánchez-Lozano, J. M., "Evaluating potential landing sites for the Artemis III mission using a multi-criteria decision making approach," *Acta Astronautica*, Vol. 226, Part 1, 2025, pp. 469–478. https://doi.org/10.1016/j.actaastro.2024.10.049.

[25] Lucas, M. P., Neal, C. R., Long-Fox, J. M., and Britt, D. T., "Simulating lunar highlands regolith profiles on Earth to inform infrastructure development and ISRU activities on the Moon," *Acta Astronautica*, Vol. 224, Nov. 2024, pp. 161–171. https://doi.org/10.1016/j.actaastro.2024.08.019.

[26] Summers, A., and Zanetti, M., "Marshall Space Flight Center: Lunar Regolith Terrain (LRT)," Poster, Marshall Jamboree & Poster Expo, Huntsville, AL, United States, May 2024. URL https://ntrs.nasa.gov/api/citations/20240004655/downloads/LRT_Jamboree_Zanetti_Poster_PrintMe.pdf, NASA Technical Reports Server (NTRS), Document ID: 20240004655.

[27] McBryan, E., Francis, P., and Sobey, A., "Dust Mitigation for the VIPER Mobility System," *54th International Conference on Environmental Systems (ICES)*, Prague, Czech Republic, 2025. URL https://ntrs.nasa.gov/api/citations/20250005201/downloads/DustMitigationfortheVIPERMobilitySystem_finalv2.pdf, NASA Technical Reports Server (NTRS) Document ID: 20250005201; Acquisition Source: Johnson Space Center; Conference dates: Jul. 13–17, 2025.

[28] National Aeronautics and Space Administration, "Classifications and Requirements for Testing Systems and Hardware to Be Exposed to Dust in Planetary Environments," Tech. Rep. NASA-STD-1008, NASA Office of the Chief Engineer, Sep. 2021. URL https://standards.nasa.gov/sites/default/files/standards/NASA/Baseline/0/2021-08-21_nasa-std-1008-approved.pdf, approved Sept. 21, 2021.

[29] Zuniga, A., Modi, H., Kaluthantrige, A., and Vertadier, H., "Building an Economical and Sustainable Lunar Infrastructure to Enable Human Lunar Missions," *International Astronautical Congress (IAC)*, Oct. 2019. URL https://ntrs.nasa.gov/api/citations/20190032258/downloads/20190032258.pdf, iAC Paper IAC-19-A5.1.7.54311; Report No. ARC-E-DAA-TN73971; NASA Technical Reports Server (NTRS) Document ID: 20190032258; Washington, DC, United States, Oct. 21–25, 2019.

[30] NASA, "VOLATILES INVESTIGATING POLAR EXPLORATION ROVER PROPOSAL INFORMATION PACKAGE," , January 2020. Rev VI. https://science.nasa.gov/wp-content/uploads/2024/08/viper-pip-final.pdf.

[31] Mottaghi, S., and Benaroya, H., "Design of a Lunar Surface Structure. II: Seismic Structural Analysis," *Journal of Aerospace Engineering*, Vol. 28, No. 1, Jan. 2015. https://doi.org/10.1061/(ASCE)AS.1943-5525.0000396.

[32] Agapkin, I., and Slyuta, E., "A review of selective laser sintering/melting techniques for lunar construction," *Acta Astronautica*, Vol. 237, 2025, pp. 315–325. https://doi.org/10.1016/j.actaastro.2025.08.047.

[33] Suggs, R., "Polar Resources Ice Mining Experiment-1 (PRIME-1) NASA's First Polar Drilling and Volatiles Detection Mission," Presentation, Space Resources Roundtable XXIII Meeting, Golden, CO, United States, June 2023. URL https://ntrs.nasa.gov/api/citations/20230007582/downloads/SRR%20PRIME-1.pdf, NASA Technical Reports Server (NTRS) Document ID: 20230007582; acquisition source: Kennedy Space Center.

[34] Granier, J., Cutard, T., Pinet, P., Le Maoult, Y., Chevrel, S., Sentenac, T., and Favier, J.-J., "Selective Laser Melting of Partially Amorphous Regolith Analog for ISRU Lunar Applications," *Acta Astronautica*, 2024. URL https://www.sciencedirect.com/science/article/pii/S0094576524005988, accessed: 2026-02-23.

[35] TRUMPF, "TruFiber P Compact (CW Fiber Laser) — Product Page," https://www.trumpf.com/en_US/products/lasers/beam-sources/cw-laser/trufiber-p-compact/, 2026. URL https://www.trumpf.com/en_US/products/lasers/beam-sources/cw-laser/trufiber-p-compact/, accessed: 2026-02-24.

[36] EKSMA Optics, "Biconcave Lenses," https://eksmaoptics.com/optical-components/lenses/biconcave-lenses/, 2026. URL https://eksmaoptics.com/optical-components/lenses/biconcave-lenses/, accessed: 2026-02-24.

[37] IDEX Optics & Photonics, "Gaussian Beam Optics," , 2023. URL https://www.idexot.com/media/wysiwyg/02_Gaussian_Beam_Optics.pdf, technical application note, Accessed: 2026-04-06.

[38] Schäfter + Kirchhoff GmbH, "Collimated Beam Diameter of a Singlemode Fiber," , 2020. URL https://www.sukhamburg.com/support/technotes/fiberoptics/coupling/collimatingsm/diameter.html, technote, Accessed: 2026-04-06.

[39] Ghasempour-Mouziraji, M., Lagarinhos, J., Afonso, D., and Sousa, R. D., "A review study on metal powder materials and processing parameters in Laser Metal Deposition," *Optics and Laser Technology*, Vol. 170, 2024, p. 110226. https://doi.org/10.1016/j.optlastec.2023.110226.

[40] Vlastos, P., Sljivo, I., Carter, C., and Woodard, A., "Developing A Dependable Multi-Agent Rover Swarm Using cFS," *WDMD 2024: 3rd International Workshop on Dependability Modeling and Design*, Oct. 2024. URL https://ntrs.nasa.gov/api/citations/20240010371/downloads/Troupe_ISSRE_WDMD_2024_2.pdf, NASA Technical Reports Server (NTRS) Document ID: 20240010371; Tsukuba, Japan; Oct. 28–31, 2024.

[41] Akshit L, "Modeling, Motion Planning, and Control of Manipulators and Mobile Robots," Clemson University, 2021. URL https://opentextbooks.clemson.edu/wangrobotics/chapter/inverse-kinematics/, accessed Feb. 26, 2026.

[42] Sayed, A., Mohamed, A., Aly, A., Hassan, Y., Abdulaziz, A., Ammar, H., and Shalaby, R., "Experimental Modeling of Hexapod Robot Using Artificial Intelligence," Nile University, 2020. URL https://biotech.nu.edu.eg/publications/experimental-modeling-hexapod-robot-using-artificial-intelligence, accessed Feb. 26, 2026.

[43] Cloud, J., Nieves, R., Duke, A., Muller, T., Janmohamed, N., Buckles, B., and Dupuis, M., "Towards Autonomous Lunar Resource Excavation via Deep Reinforcement Learning," NASA, Nov 2021. URL https://ntrs.nasa.gov/citations/20210022218, accessed Feb. 26, 2026.

A. Appendix A: Requirements List

Rquirement ID	Requirement	Rquirement ID	Requirement
R-MIS-010	LSRH shall autonomously create a small-size LLP suitable for landing small missions on the lunar surface that will facilitate the construction of a lunar base. This will be accomplished incrementally with 1-meter wide hexagonal tiles.	R-LAS-010	A fiber optic laser shall be used to sinter lunar regolith material and construct lunar landing pads.
R-MIS-020	LSRH shall prove the feasibility of a hexapod mobility system on the lunar surface.	R-LAS-020	Optical power for the fiber optic laser shall have variable power settings between 2000W and 3000W at a wavelength between 1060 and 1080 nanometers.
R-MIS-030	LSRH shall fit within the allocated space on the Griffin Lander.	R-LAS-030	Regolith will be sintered between 670 and 1150 degrees Celsius with a target temperature range between 820-850 degrees Celsius to ensure crystallization and annealing of regolith without melting
R-MIS-040	All performance and functional requirements shall be met in a vacuum chamber that emulates the lunar vacuum environment. Testing shall be performed in the Environmental Test Facility (ETF) at Marshall Space Flight Center (MSFC).	R-LAS-040	Scan speed shall vary between 5 mm/s and 320 mm/s to optimize energy delivered and quality of processed regolith.
R-MIS-050	All LSRH components shall comply with the NASA-STD-1008 dust mitigation standard.	R-LAS-050	Hatch spacing shall match the spot diameter of the laser to ensure connection of sintered tiles.
R-MIS-060	The laser sintering device shall be verified by sintering an appropriate lunar regolith stimulant such as LSP-2 or LHS-2. The compression strength shall be tested and must be at least 4.2 MPa.	R-LAS-060	Surface Energy Density shall be greater than 0.9 J/mm^2 to ensure compressive strength of the regolith is greater than 4.2MPa; this can be achieved by varying powerand scan speed.
R-MIS-070	The LSRH will undergo component and system functional testing before and after vibration testing to ensure survival of launch conditions.	R-LAS-070	Laser housing shall operate between 10 and 40 degrees Celsius to prevent overheating of diode module.
R-MIS-080	A prototype of the LSRH will be constructed during the early development period to assess system performance.	R-GNC-010	The LSRH GN&C system will monitor other subsystems and distribute commands to maintain the operation of the LSRH within prescribed limits.
R-LAD-010	The delivery vehicle shall be the Astrobotic Griffin Lunar Lander.	R-GNC-020	The central computer of the LSRH will serve as the central control point for all commands.
R-LAD-020	The LSRH shall survive launch and transport to the lunar surface.	R-GNC-030	The LSRH shall define its location on the moon using coordinate tracking. LiDAR will be used to visually map the lunar surface and enable autonomous obstacle navigation.
R-PLD-010	The fiber optic laser shall harden the lunar surface by sintering the regolith.	R-GNC-040	An external temperature monitor shall observe the sintering process and relay the surface temperature of sintered regolith.
R-PLD-020	The robotic arm shall contain the laser sintering device and provide a stable platform for thermal imaging and sintering regolith.	R-GNC-050	The external regolith temperature monitor shall have a measurement range between 300 K and 1500K.
R-MOB-010	The hexapod system shall enable the LSRH to execute mobility commands from the onboard computer, deploy from the Griffin lander and maneuver around the lunar surface, and maneuver adequately to accomplish landing pad construction.	R-GNC-060	A collection of internal temperature monitors onboard the LSRH shall regularly report temperature levels around sensitive components to the main computer.
R-MOB-020	The hexapod mobility system shall have a latency of less than 10 ms between onboard autonomous computer commands and physical motion.	R-GNC-070	An internal sensor complex shall record the rover's stability, reporting data to the central computer to prevent mission failure due to loss of stability.
R-MOB-030	The hexapod legs shall have a step error of less than 5 mm between intended input and actual physical step location.	R-COM-010	The LSRH communication relay system shall be compatible with the 2.4 GHz IEEE 802.11n compliant WLAN modem contained onboard the Griffin Lunar Lander.
R-MOB-040	The hexapod mobility system shall propel the rover and support a mass of up to 200kg.	R-THM-010	The LSRH thermal regulation system shall maintain highly sensitive internal components between -20ºC and 50ºC.
R-MOB-050	The mobility system shall propel the rover at a cost of transport below 4.00.	R-PWR-010	The LSRH shall receive power from the Griffin Lunar Lander through a tethered connection.
R-MOB-060	The mobility system shall keep the LSRH stable up to a slope angle of 30 degrees on the lunar surface.	R-SAF-010	Automated or robotic systems shall provide any human operator the ability to safely override and shut down automated systems or subsystems
R-MOB-070	The mobility system shall demonstrate sustained stable transport on NASA Marshall Space Flight Center Lunar Regolith Terrain prior to launch.	R-SAF-020	Automated or robotic systems shall provide any human operator with a range of control options that accommodates the expected operating conditions

Fig. 20 Screenshot of Requirements List